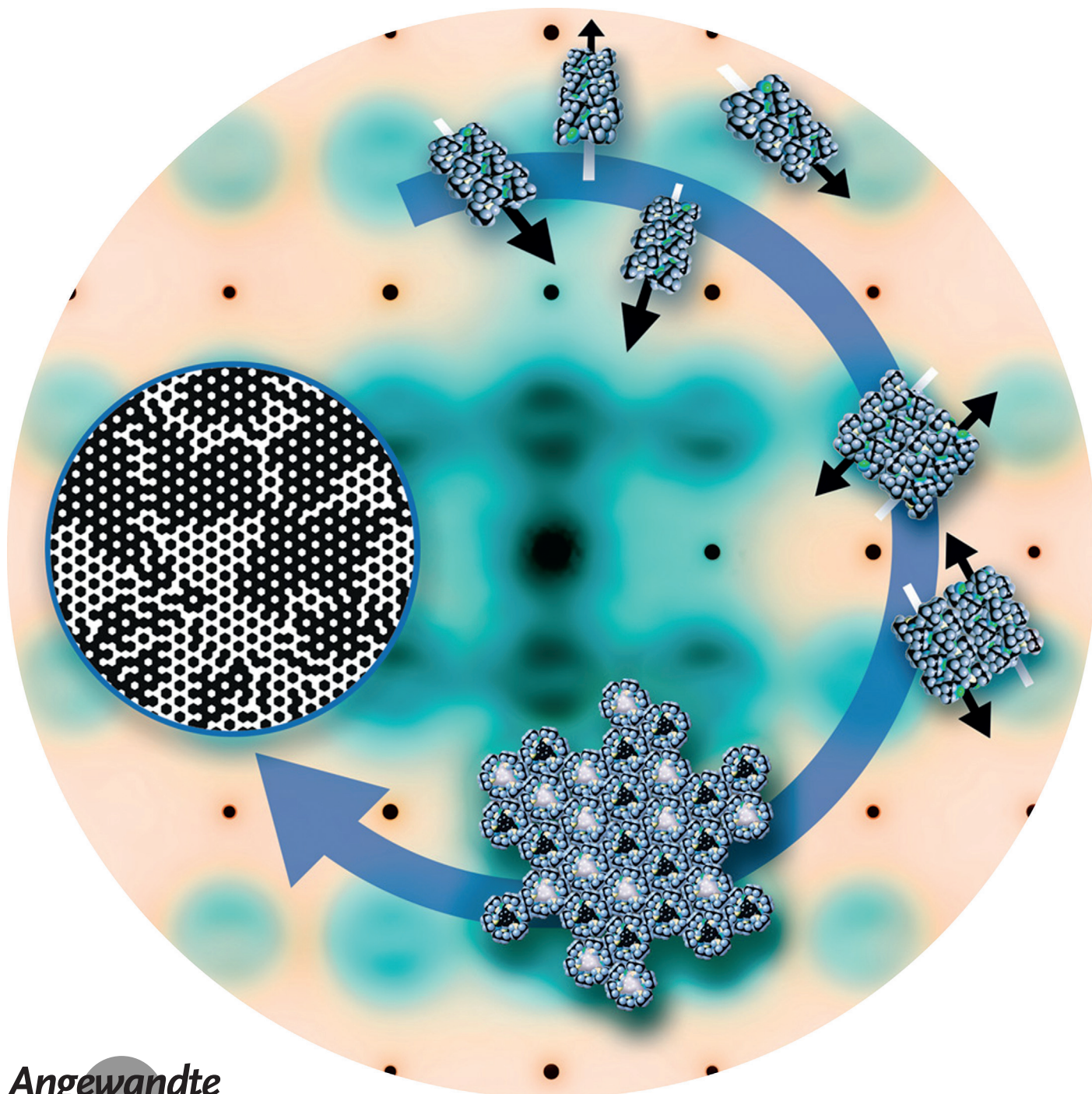


Organic Ferroelectrics

International Edition: DOI: 10.1002/anie.201612122
German Edition: DOI: 10.1002/ange.201612122

Mesoscale Polarization by Geometric Frustration in Columnar Supramolecular Crystals

Christoph S. Zehe, Joshua A. Hill, Nicholas P. Funnell, Klaus Kreger, Kasper P. van der Zwan, Andrew L. Goodwin,* Hans-Werner Schmidt,* and Jürgen Senker*



Abstract: Columnar supramolecular phases with polarization along the columnar axis have potential for the development of ultrahigh-density memories as every single column might function as a memory element. By investigating structure and disorder for four columnar benzene-1,3,5-trisamides by total X-ray scattering and DFT calculations, we demonstrate that the column orientation, and thus the columnar dipole moment, is receptive to geometric frustration if the columns aggregate in a hexagonal rod packing. The frustration suppresses conventional antiferroelectric order and heightens the sensitivity towards collective intercolumnar packing effects. The latter finding allows for the building up of mesoscale domains with spontaneous polarization. Our results suggest how the complex interplay between steric and electrostatic interactions is influenced by a straightforward chemical design of the molecular synthons to create spontaneous polarization and to adjust mesoscale domain size.

Organic materials featuring ferroelectric polarization^[1] are attractive candidates for easily processable and low-cost electric sensors,^[2] electro-optics,^[3] as well as non-volatile memory devices.^[4] The fundamental requirement for these materials is spontaneous and switchable polarization. In supramolecular solids^[1,3] and liquid crystalline (LC) phases,^[5] the latter is generally induced by ordering either permanent molecular dipoles or supramolecular dipole moments that are generated or enhanced by the assembly.^[6] In particular, materials with polarization along the columnar axis (referred to as axially polar) have gained increasing interest owing to their potential applicability for ultrahigh-density memories, where individual columns might ultimately act as memory elements.^[7,8]

Recently, the first example of an intrinsically ferroelectric, axially polar LC with a remnant polarization of $1.7 \mu\text{C cm}^{-2}$ was obtained by columnar stacking of a phthalonitrile derivative.^[9] Kemerink, Sijbesma, and co-workers reported a sim-

ilar polarization of up to $2 \mu\text{C cm}^{-2}$ for thin films of oriented LCs^[10] that consisted of benzene-1,3,5-trisamides (BTAs)^[11] with long aliphatic side groups. Although the polarization could be induced and switched by electric fields, its stabilization was only possible by freezing the LC state.^[10,11] Therefore, one of the biggest challenges for axially polar materials remains the creation and control of spontaneous polarization in the absence of external stimuli. The latter requires the counterbalance of the electrostatic interactions between the dipoles of neighboring columns in a side-by-side arrangement, which inevitably favors an *anti* alignment of the columnar polarization, resulting in non-polar phases.^[3] Hence, suitable columnar materials with spontaneous and stable polarization are rare up to now, and for the few observed cases,^[8] its emergence remained unexplained.^[7-9,12-14]

Herein, we present a structural study of four purposely synthesized BTAs with the aim of investigating the origin of spontaneous polarization for axially polar systems in their solid state, which offers the unique possibility to study dipole order governed solely by intrinsic interactions. In general, BTAs are based on a benzene core that is linked to peripheral groups via three amide bonds in the 1-, 3-, and 5-positions (Figure 1a). The formation of threefold intermolecular hydrogen bonds in a helical arrangement drives the molecular self-assembly into well-ordered columns (Figure 1b, left), in which all carbonyl bonds are aligned in the same direction along the columnar axis. The individual dipole moments of these bonds add up to macrodipoles^[10] along the columnar axis (Figure 1b, left). In a side-by-side arrangement of two columns, the electrostatic interactions prefer an *anti* alignment of the macrodipoles (Figure 1c). Simultaneously, the peripheral groups give rise to a corrugated surface topography for the supramolecular aggregates (Figure 1b, right), imposing steric restraints (Figure 1c) that may favor parallel or antiparallel arrangements depending on subtle structural details of the peripheral groups. As van der Waals forces favor dense packings of neighboring columns, hexagonal rod packings^[14] are often induced (Figure 1d). In such packings, however, the macrodipole interaction between neighboring columns becomes frustrated as it is not possible to simultaneously align all dipoles antiparallel relative to their nearest neighbors (Figure 1d). This frustration reduces the contribution of the macrodipole interactions to the lattice energy and thus amplifies the influence of steric restraints. If the latter favors the parallel alignment of neighboring columns, stable ferroelectric domains should be feasible for axially polar materials.

Based on this model, compounds **1–4** (Figure 2a) were selected, for which we expected a varying ratio of macrodipole and steric interactions. Single crystals were grown either by solvent evaporation or by sublimation and analyzed by single-crystal X-ray diffraction (for crystallographic details, see the Supporting Information, Section S2). All four BTAs crystallize in hexagonal rod packings (Figure 2b), which is in agreement with previous studies on **1**^[15] and **2**.^[16] Whereas **1**, **2**, and **4** exhibit similar intercolumnar distances d_{cc} of 14.1 Å, 14.5 Å, and 13.9 Å, the longer peripheral groups of **3** increase the d_{cc} value to 17.1 Å. The C=O centered linkages of **1** and **3**

[*] Dr. C. S. Zehe, K. P. van der Zwan, Prof. Dr. J. Senker
Inorganic Chemistry III, University of Bayreuth
Universitätsstrasse 30, 95447 Bayreuth (Germany)
E-mail: juergen.senker@uni-bayreuth.de

Dr. J. A. Hill, Dr. N. P. Funnell, Prof. Dr. A. L. Goodwin
Department of Chemistry, University of Oxford
Inorganic Chemistry Laboratory
South Parks Road, Oxford OX1 3QR (UK)
E-mail: andrew.goodwin@chem.ox.ac.uk

Dr. N. P. Funnell
Current address: ISIS, Rutherford Appleton Laboratory
Chilton, Didcot OX11 0QX (UK)

Dr. K. Kreger, Prof. Dr. H.-W. Schmidt
Macromolecular Chemistry I, University of Bayreuth
Universitätsstrasse 30, 95447 Bayreuth (Germany)
E-mail: hans-werner.schmidt@uni-bayreuth.de

Supporting information and the ORCID identification number(s) for the author(s) of this article can be found under:
<http://dx.doi.org/10.1002/anie.201612122>.

© 2017 The Authors. Published by Wiley-VCH Verlag GmbH & Co. KGaA. This is an open access article under the terms of the Creative Commons Attribution License, which permits use, distribution and reproduction in any medium, provided the original work is properly cited.

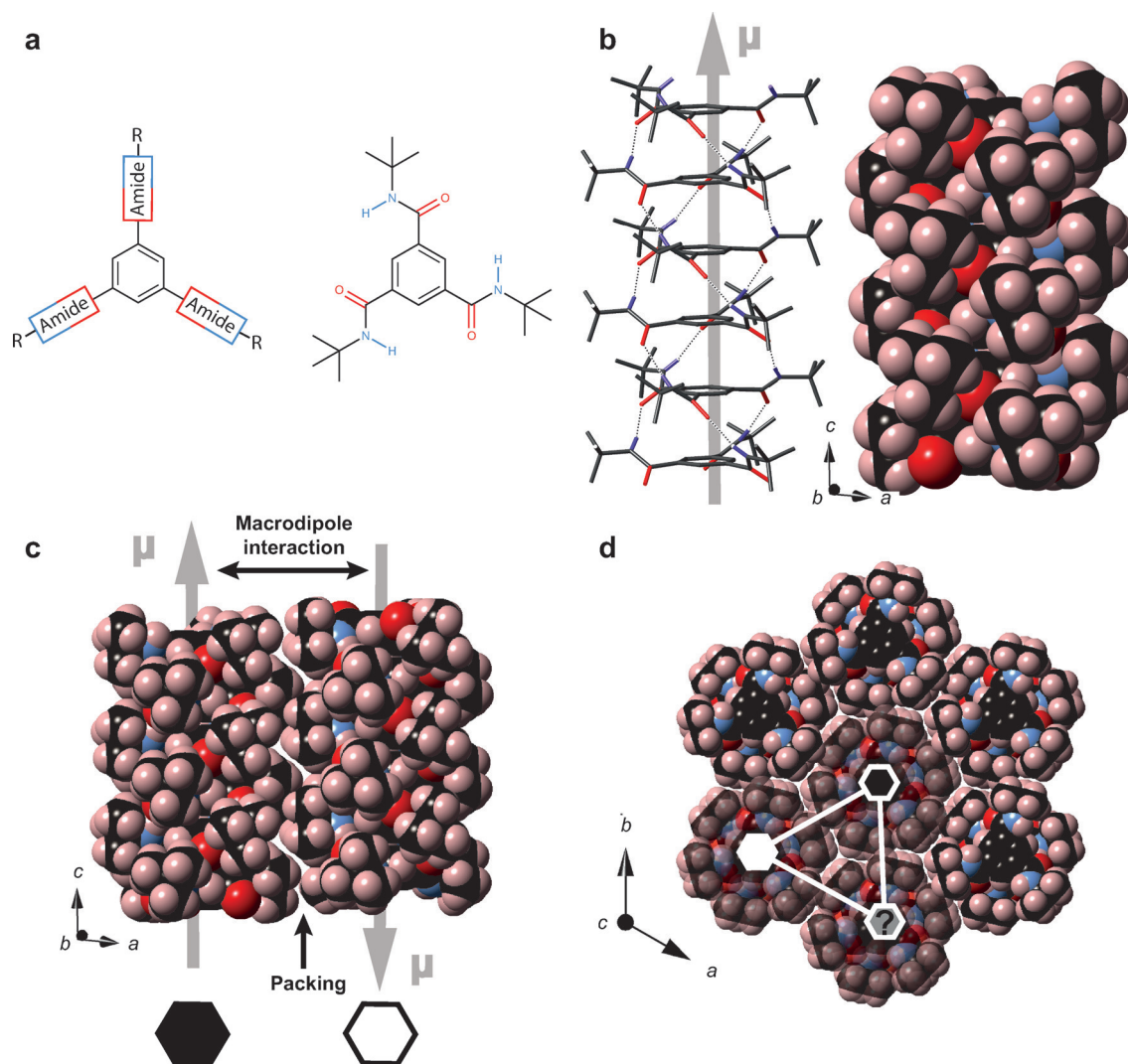


Figure 1. a) Basic design scheme of BTAs, which consist of a benzene core linked to peripheral groups R (such as *tert*-butyl moieties) via amide bonds in the 1-, 3-, and 5-positions. b) Side view of a columnar stack of six BTA molecules (left); the hydrogen bonds are indicated as dotted lines (all non-NH protons omitted for clarity). The macrodipole is highlighted as a gray arrow. A space-filling model of the same stack is depicted on the right. c) Side view of two columns in antiparallel orientation, where the direction of the macrodipole is symbolized by black and white hexagons. d) Top view of an ensemble of seven stacks in hexagonal rod packing indicating possible geometric frustration.

feature higher torsional flexibility of the amide groups with mean side-chain torsions of $\Phi(\text{C}_{\text{ar}}\text{C}_{\text{ar}}\text{C}_{\text{O}}\text{O}) \approx 39.5^\circ$ (**1**) and 34.6° (**3**) compared to the N-centered systems with $\Phi(\text{C}_{\text{ar}}\text{C}_{\text{ar}}\text{C}_{\text{O}}\text{O}) \approx 35.1^\circ$ (**2**) and 23.7° (**4**). Larger torsion angles cause a steeper inclination of the C=O bonds towards the columnar axis and will thus lead to larger macrodipoles.

To derive a more quantitative picture of the macrodipole strengths, we estimated the average molecular dipole moments p representative for the columnar dipole for the smaller molecules **1**, **2**, and **4** by quantum-chemical calculations on finite clusters taken from the single-crystal structure solutions (Section S3). In line with the structural considerations, p amounts to 12 D and 11 D for **1** and **2**, respectively, and to 6.5 D for **4**. For the latter, the p value is reduced further because of the *anti* alignment of the C–F and C=O bonds, which is induced by intramolecular NH \cdots F hydrogen bonds (Figure 2a,b and Figure S4b).^[17] In the

case of **3**, we expect a value close to the one derived for **2** as their mean torsion angles are similar. As a consequence, the strongest macrodipole interactions arise for **1** ($p = 12$ D, $d_{\text{cc}} = 14.1$ Å), closely followed by **2** (11 D, 14.5 Å) and a significant reduction for **3** (11 D, 17.1 Å) owing to the larger d_{cc} value and **4** (6.5 D, 13.9 Å) based on the smaller p value.

Remarkably, for **1**,^[15] **2**, and **3**, each stack appears as a superposition of two columns with opposite macrodipole orientations in the conventional structure solution (Figure 2c). As Bragg diffraction arises from spatially averaged electron density within the coherence length of the X-ray beam (ca. 100 nm), this reflects disorder of the macrodipole orientations in individual unit cells.^[18] For **1**, both orientations are equally present (Figure 2c), and hence on average, each stack has a 50% probability to be either in the up or the down state. In contrast, we observed superstructures with a stripe-

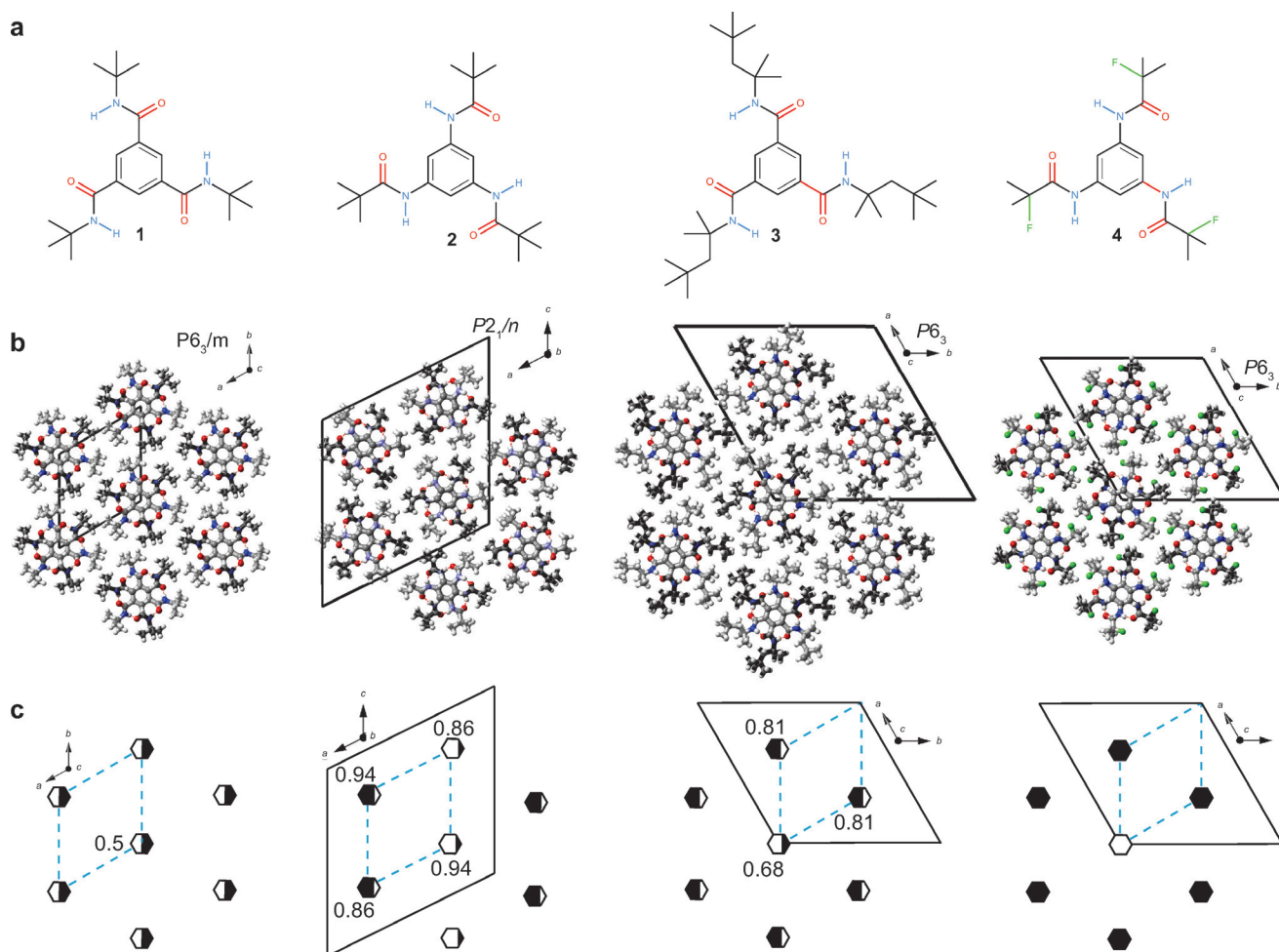


Figure 2. a) BTA molecules **1–4**. b) Bragg structure solutions viewed along the direction of the molecular stacks, coinciding with the direction of the polar axes of the indicated space groups. c) Schematic representation of the probabilities for up- and down-oriented columns within one stack (major components displayed), which are additionally symbolized by the amount of black and white in each hexagon. The dashed blue lines indicate the unit cells of the underlying hexagonal or pseudo-hexagonal (in the case of **2**) lattices whereas the black solid lines demarcate the unit cells found by single-crystal X-ray diffraction.

type macrodipole arrangement for **2** and with a honeycomb pattern for **3** and **4** (Figure 2c). For the latter BTAs, in each stack, one particular column orientation is more likely than the other as indicated by the color code presented in Figure 2c. Nevertheless, the unit cells of **1** and **2** contain no net macrodipole moment as equal amounts of up- and down-oriented columns are present. For **3** and **4**, the unit cells contain an excess of one orientation, which leads to a net polarization along the direction of the columnar axis.

In addition to the sharp Bragg reflections, selected layers of reciprocal space exhibit intense, structured, diffuse scattering for compounds **1**, **2**, and **3** (Figure 3a).^[18] In all cases, the diffuse intensities are confined to layers perpendicular to the stacking direction (Figure S2). The diffuse scattering explains the disorder for up- and down-oriented columns as described above (Figure 2c) and suggests deviations from the average structures for neighboring columns within a coherence length below 100 nm. In contrast, the columns are rather well-ordered along the stacking direction on significantly larger length scales. To develop models that reproduce the observed

diffuse scattering pattern, we found it to be sufficient to position supramolecular columns in a hexagonal rod packing, with only the up and down orientation of the macrodipoles subject to disorder, while the packing along the stacking direction is ordered over the whole column. We then predicted the ferroelectric and antiferroelectric alignments of neighboring macrodipoles based on a 2D Ising model.^[19] Here, the energy of the system is defined based on two effective coupling constants J_1 and J_2 , which describe the sum of both the electrostatic and steric interactions between nearest neighbor (n.n.) and next-nearest neighbor (n.n.n.) columns.^[19] J_1 and J_2 are subsequently varied until the best match between the simulated and experimental diffraction patterns (Figure 3a,b) is reached (for a description of the technical procedure, see Section S1.4).

The resulting arrangements of up- and down-oriented macrodipoles (Figure 3c) reproduce the diffuse scattering pattern (Figure 3a) with almost perfect agreement. **1** and **2** both exhibit disorder on a local scale with preferential stripe-type antiferroelectric arrangements between neighboring

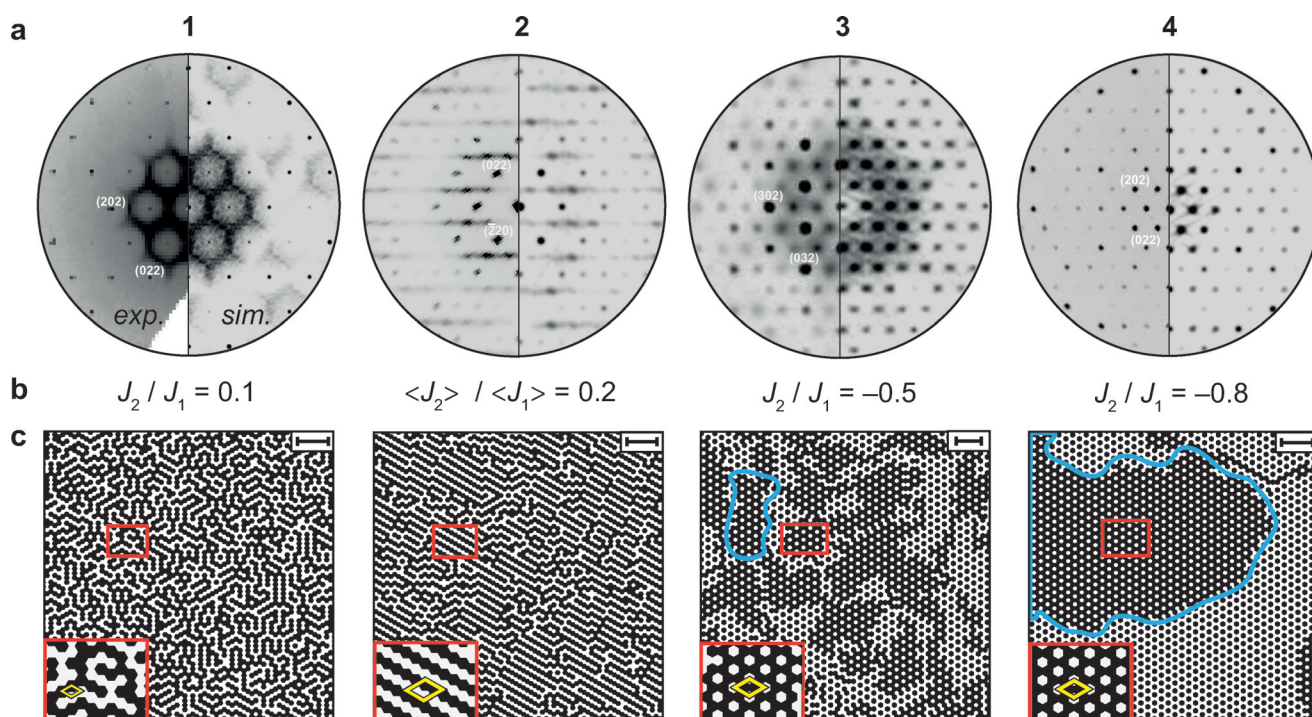


Figure 3. a) The $(hk2)$ planes for **1**, **3**, and **4** and the $(h2k)$ plane for **2** of reconstruction of the reciprocal space, together with simulations (experimental picture of **1** taken from Ref. [15]). These planes are perpendicular to the stacking direction. b) Ratios for the refined coupling constants J_1 and J_2 of the Ising model simulations for **1–4**. Owing to the reduced crystallographic symmetry in the case of **2**, average values are given (Figure S1). All constants were normalized according to $J_1/kT = 1$, with T being the simulation temperature. c) Resulting arrangement of up- and down-oriented macrodipoles over approximately 70×70 columns. The red boxes contain magnifications of local features, and the crystallographic unit cells are indicated in yellow (Figure 2b). The blue lines emphasize domains exhibiting net polarization for **3** and **4**. The scale bars in the top right corners correspond to a distance of 10 nm.

columns. In contrast, for **3** and **4**, mesoscale domains with a honeycomb structure carrying spontaneous polarization are formed. While the average domain size is on the order of 20–30 nm for **3**, the domains become significantly larger (50–70 nm) for **4**. Furthermore, the excellent match between the observed and simulated X-ray powder diffraction data (Figures S5–S8) demonstrates that both the disorder and the mesoscale domain formation are inherent properties of the bulk materials. Although domains with spontaneous polarization have been suggested for axially polar phases before,^[7–9,12,20] our data provide the first experimental evidence for their existence. For such small domains, other common methods, such as the second harmonic generation effect, are inconclusive^[21] or change the domain structure as for pyroelectric measurements. In our case, total scattering proves to be the method of choice for probing small domains without affecting the spontaneous polarization.

For the two compounds with the larger macrodipole interactions (**1** and **2**), both J_1 and J_2 are positive, indicating that the electrostatic interaction, and thus an antiferroelectric alignment between n.n. and n.n.n. columns, dominates. This inevitably leads to disorder for up- and down-oriented columns on local length scales and non-polar unit cells (Figure 2c and Figure 3c). In contrast, for **3** and **4**, where the electrostatic interaction is significantly reduced, J_1 and J_2 bear opposite signs with $J_1 > 0$ and $J_2 < 0$. Consequently, only n.n. columns tend to be *anti*-aligned while n.n.n. stacks

favor a parallel alignment. The latter occurs only when the steric interactions and collective packing effects^[22] become stronger than the electrostatic forces. The tendency for an opposite alignment for n.n. and n.n.n. columns in turn is the origin of the formation of mesoscale domains with spontaneous polarization and polar unit cells (Figure 2c and Figure 3c). Based on the calculated molecular dipole moments, the polarization within these domains reaches values of $1.6 \mu\text{C cm}^{-2}$ and $1.4 \mu\text{C cm}^{-2}$ for **3** and **4**, which are among the largest values obtained for axially polar phases to date.^[9–13,23]

Established approaches for creating ferroelectric order make use of supramolecular interactions between individual molecules to counteract the electrostatic interaction.^[3] In contrast, we have shown that for axially polar phases, polarization emerges from weak steric interactions between self-assembled supramolecular columns if the systems are prone to geometric frustration. As these interactions are encoded in the molecular structure, the latter drive the dipole ordering and the length scale of domain formation. As such, it is possible to move between nonpolar stripe-type and polar honeycomb phases in a 2D Ising phase diagram (Figure 4).^[19] Our finding illustrates emerging complexity^[24] and is an intriguing example of introducing hierarchical order in supramolecular systems.^[25] With small, but systematic chemical modifications of the molecular synthons, a broad range of antiferroelectric and ferroelectric domain structures are accessible. Counterintuitively, mesoscale domains are maxi-

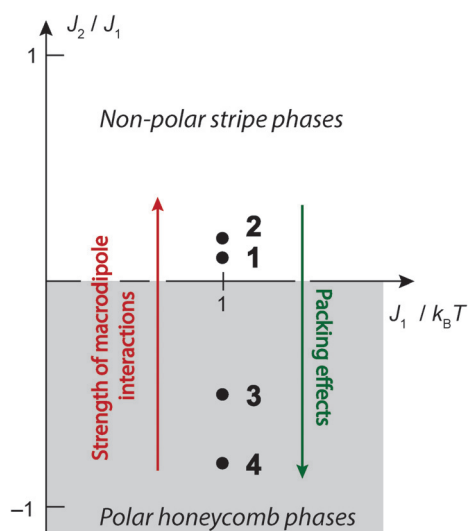


Figure 4. The ground-state phase diagram^[19] of the simple 2D Ising model exhibiting antiferroelectric nearest ($J_1 > 0$) and varying next-nearest neighbor interactions.

mized for systems where dipolar interactions are reduced. Following this idea for other columnar materials may lead to the development of a wide variety of solid and liquid-crystalline, axially polar columnar ferroelectric materials.

Acknowledgements

C.S.Z., K.P.Z., H.-W.S., and J.S. gratefully acknowledge financial support from the German Research Foundation (SFB 840). Furthermore, we thank the Hanns-Seidel-Foundation (C.S.Z.) and the Elite Network Bavaria (C.S.Z. and K.P.Z.) for financial and other support. All authors thank Thomas Weber (ETH Zürich) for the crystal-structure data of **1** and Sandra Ganzleben for her support with the syntheses of the compounds. A.L.G., J.A.H., and N.P.F. gratefully acknowledge financial support from the ERC (Grant 279705) and the EPSRC (Grant EP/G004528/2).

Conflict of interest

The authors declare no conflict of interest.

Keywords: Ising model · organic ferroelectrics · self-assembly · supramolecular chemistry · total X-ray scattering

How to cite: *Angew. Chem. Int. Ed.* **2017**, *56*, 4432–4437
Angew. Chem. **2017**, *129*, 4502–4508

- [1] S. Horiuchi, Y. Tokura, *Nat. Mater.* **2008**, *7*, 357–366.
- [2] J. F. Scott, *Science* **2007**, *315*, 954–959.
- [3] A. S. Tayi, A. Kaeser, M. Matsumoto, T. Aida, S. I. Stupp, *Nat. Chem.* **2015**, *7*, 281–294.
- [4] K. Asadi, D. M. de Leeuw, B. de Boer, P. W. M. Blom, *Nat. Mater.* **2008**, *7*, 547–550.
- [5] S. T. Lagerwall, *Ferroelectrics* **2004**, *301*, 15–45.
- [6] a) S. Horiuchi, F. Ishii, R. Kumai, Y. Okimoto, H. Tachibana, N. Nagaosa, Y. Tokura, *Nat. Mater.* **2005**, *4*, 163–166; b) D.-W. Fu et al., *Science* **2013**, *339*, 425–428; c) S. Horiuchi, Y. Tokunaga, G. Giovannetti, S. Picozzi, H. Itoh, R. Shimano, R. Kumai, Y. Tokura, *Nature* **2010**, *463*, 789–792; d) S. Horiuchi, Y. Okimoto, R. Kumai, Y. Tokura, *Science* **2003**, *299*, 229–232; e) E. Collet et al., *Science* **2003**, *300*, 612–615; f) A. S. Tayi et al., *Nature* **2012**, *488*, 485–489.
- [7] K. Kishikawa, S. Nakahara, Y. Nishikawa, S. Kohmoto, M. Yamamoto, *J. Am. Chem. Soc.* **2005**, *127*, 2565–2571.
- [8] H. Takezoe, K. Kishikawa, E. Gorecka, *J. Mater. Chem.* **2006**, *16*, 2412–2416.
- [9] D. Miyajima, F. Araoka, H. Takezoe, J. Kim, K. Kato, M. Takata, T. Aida, *Science* **2012**, *336*, 209–213.
- [10] C. F. C. Fitié, W. S. C. Roelofs, M. Kemerink, R. P. Sijbesma, *J. Am. Chem. Soc.* **2010**, *132*, 6892–6893.
- [11] S. Cantekin, T. F. A. de Greef, A. R. A. Palmans, *Chem. Soc. Rev.* **2012**, *41*, 6125–6137.
- [12] H. Zimmermann, R. Poupko, Z. Luz, J. Billard, *Z. Naturforsch.* **1985**, *40*, 149–160.
- [13] C. Tschierske, *Nature* **2002**, *419*, 681–683.
- [14] M. O’Keeffe, S. Andersson, *Acta Crystallogr. Sect. A* **1977**, *33*, 914–923.
- [15] M. Kristiansen, P. Smith, H. Chanzy, C. Baerlocher, V. Gramlich, L. McCusk, T. Weber, P. Pattison, M. Blomenhofer, H.-W. Schmidt, *Cryst. Growth Des.* **2009**, *9*, 2556–2558.
- [16] M. Schmidt, J. Wittmann, R. Kress, D. Schneider, S. Steuernagel, H.-W. Schmidt, J. Senker, *Cryst. Growth Des.* **2012**, *12*, 2543–2551.
- [17] C. Zehe, M. Schmidt, R. Siegel, K. Kreger, V. Daebel, S. Ganzleben, H.-W. Schmidt, J. Senker, *CrystEngComm* **2014**, *16*, 9273–9283.
- [18] D. A. Keen, A. L. Goodwin, *Nature* **2015**, *521*, 303–309.
- [19] U. Brandt, J. Stolze, *Z. Phys. B* **1986**, *64*, 481–490.
- [20] E. Gorecka, D. Pocięcha, J. Mieczkowski, J. Matraszek, D. Guillon, B. Donnio, *J. Am. Chem. Soc.* **2004**, *126*, 15946–15947.
- [21] J. Breu, P. Stössel, S. Schrader, A. Starukhin, W. J. Finkenzeller, H. Yersin, *Chem. Mater.* **2005**, *17*, 1745–1752.
- [22] T. R. Welberry, A. P. Heerdegen, D. C. Goldstone, I. A. Taylor, *Acta Crystallogr. Sect. B* **2011**, *67*, 516–524.
- [23] a) A. Sugita, K. Suzuki, S. Tasaka, *Chem. Phys. Lett.* **2004**, *396*, 131–135; b) H. Pleiner, H. R. Brand, P. E. Cladis, *Mol. Cryst. Liq. Cryst.* **2003**, *396*, 169–176.
- [24] A. B. Cairns, M. J. Cliffe, J. A. M. Paddison, D. Daisenberger, M. G. Tucker, F.-X. Coudert, A. L. Goodwin, *Nat. Chem.* **2016**, *8*, 442–447.
- [25] T. Aida, E. W. Meijer, S. I. Stupp, *Science* **2012**, *335*, 813–817.

Manuscript received: December 13, 2016
Final Article published: March 20, 2017